

Thick CrN/NbN Multilayer Coating Deposited by Cathodic Arc Technique

Juliano Avelar Araujo^a, Roberto Martins Souza^b, Nelson Batista de Lima^c, André Paulo Tschiptschin^{a,d,*}

^a Metallurgical and Materials Engineering Department, University of São Paulo – USP, Av. Prof. Mello Moraes, 2463, ZIP 05508-030, São Paulo, SP, Brazil

^b Mechanical Engineering Department, University of São Paulo – USP, Av. Prof. Mello Moraes, 2231, ZIP 05508-030, São Paulo, SP, Brazil

^c Department of Materials Characterization, Nuclear and Energy Research Institute – IPEN, Av. Prof. Lineu Prestes, 2242, CEP 05508-900, São Paulo, SP, Brazil

^d Brazilian Nanotechnology National Laboratory – LNNano, Brazilian National Center of Research in Energy and Materials – CNPEM, Rua Giuseppe Maximo Scolfaro, 10000, CEP 13083-100, Campinas, SP, Brazil

Received: April 10, 2016; Revised: October 25, 2016; Accepted: November 21, 2016

The production of tribological nanoscale multilayer CrN/NbN coatings up to 6 μm thick by Sputtering/HIPIMS has been reported in literature. However, high demanding applications, such as internal combustion engine parts, need thicker coatings ($>30 \mu\text{m}$). The production of such parts by sputtering would be economically restrictive due to low deposition rates. In this work, nanoscale multilayer CrN/NbN coatings were produced in a high-deposition rate, industrial-size, Cathodic Arc Physical Vapor Deposition (ARC-PVD) chamber, containing three cathodes in alternate positions (Cr/Nb/Cr). Four 30 μm thick NbN/CrN multilayer coatings with different periodicities (20, 10, 7.5 and 4 nm) were produced. The coatings were characterized by X-Ray Diffraction (XRD) and Transmission Electron Microscopy (TEM). The multilayer coating system was composed of alternate cubic rock-salt CrN and NbN layers, coherently strained due to lattice mismatch. The film grew with columnar morphology through the entire stratified structure. The periodicities adopted were maintained throughout the entire coating. The 20 nm periodicity coating showed separate NbN and CrN peaks in the XRD patterns, while for the lower periodicity ($\leq 10\text{nm}$) coatings, just one intermediate lattice (d-spacing) was detected. An almost linear increase of hardness with decreasing bilayer period indicates that interfacial effects can dominate the hardening mechanisms.

Keywords: NbN/CrN, Multilayer Coatings, Cathodic Arc, Nanostructure

1. Introduction

The CrN is a classic coating system, which is technologically relevant since the early 1980's¹⁻⁵. The high hardness and lower friction coefficient, when compared to other piston ring system coatings^{2,6,7}, has drawn engineer's attention to the use of this kind of coating for internal combustion engine components. Currently, it is applied in large scale for piston rings^{2,5}. While typical applications may not require the PVD coating thickness to be above 6 μm ⁵, it frequently needs to be on the order of 30 μm when the PVD layer is deposited onto a combustion engine component⁵⁻⁷. Such high thickness is mandatory when considering the highly demanding environment of internal combustion engines, which is associated to high wear rates⁸. Furthermore, the increasing combustion pressures and the reduced lubrication oil availability found in new generation engines require additional toughness and wear resistance to avoid damage of the parts.

In recent years, multilayer CrN/NbN coatings have attracted Engineer's attention, since the niobium nitride

component (NbN) stands out for its chemical stability⁸ and the chromium nitride (CrN) is a hard and inert coating component^{2,3}, offering the temperature resistance required for working in the combustion chamber environment. NbN/CrN nanostructured multilayer coating combines high hardness with chemical stability and toughness. Besides that, Munz *et al.*⁹ have reported a superior wear resistance of CrN/NbN multilayer coatings over single layer coatings and electrodeposited chromium. Most of CrN/NbN coatings studied were produced by sputtering process, with or without an interlayer produced by cathodic arc evaporation¹⁰⁻¹⁴. In a few cases¹⁵, the coatings were entirely produced by the cathodic arc technique, as in this work. Many CrN/NbN PVD coatings described in the literature are up to 6 μm thick, which makes them inappropriate for applications that require long-term high wear resistance, such as internal combustion engine parts. The issues in achieving larger thicknesses using sputtering include the difficulty in keeping the multilayer periodicity through the entire coating, due to target poisoning. Many authors have studied the relationship between structure and mechanical properties of different PVD sputtered multilayer coatings with typical thickness

* e-mail: antschip@usp.br

between 2-5 μm , relating such properties to the periodicity (Λ) and the interface morphology^{12,16-18}.

Hovsepian *et al.*¹⁹⁻²¹, Munz *et al.*^{9,12} and Tomlinson *et al.*¹⁴ have reported the characterization of multilayer CrN/NbN coatings, particularly pointing out the advantages of using arc bond sputtering (ABS). The results showed that the position of CrN and NbN X-ray diffraction peaks represented the weighted mean of the individual reflections of the CrN and NbN phases. According to the authors, the occurrence of satellite peaks demonstrated the superlattice nature of the coating structure. Additionally, Hovsepian *et al.*²² produced CrN/NbN by three different PVD techniques (ABS, UBM and ARC) and showed that, despite the low bias voltage of ARC process, there is an increase in ion energy up to 300 eV. This value resulted in an increased adatom mobility, when compared to 120 eV for UBM, which suppresses interface roughness effects and may produce a smoother interface between individual CrN or NbN layers. CrN/NbN deposited by ARC showed the lowest friction coefficient and highest wear resistance, when compared to CrN/NbN produced by sputtering processes.

Lewis *et al.*²³ grew CrN/NbN by UBM in different bias voltages and found up to 14% reduction in periodicity throughout the multilayer in coatings 1.4 μm thick. The reduction was consistent for 3.0 μm thick coatings as well. The periodicity reduction was justified by the increase of target poisoning with time.

Wang *et al.*^{24,25} studied the corrosion and wear resistance of NbN/CrN coatings produced by ABS. They showed that the coating must be substantially thicker than the size of the macroparticles causing wear, in order to mitigate their effects on the NbN/CrN coating performance.

Pecchio¹⁵, Bemporad¹³, Ceschini²⁶, Martini²⁷ and Piloni²⁸ have studied NbN/CrN coatings entirely produced by arc processes. These coatings were produced using the switch cathodic arc evaporation technique, which is characterized by alternate triggering of the Cr or Nb cathodes. These coatings showed better wear performance than CrN single-material coatings produced by the same process.

It is important to notice that the research works mentioned above were centered on coatings with thickness lower than 6 μm . In terms of deposition processes, cathodic ARC has industrial interest due to its high deposition rate when compared to sputtering. The later would be economically restrictive when one compares the deposition rate of Sputtering/HIPIMS ($\sim 1.2 \mu\text{m/hr}$)^{23,29} with ARC ($\sim 3.0 \mu\text{m/hr}$)¹³.

This work explored and found features never presented before. One example is the high coating thickness - in the order of 30 μm , since coatings with such thickness were reported only in a previous work by the authors³³. In addition to the technological benefit, extending service life of components, the thick coatings in this work allowed exploring some features of the cathodic arc technique such as the evolution of the coating structure during the deposition process. In this case,

the results confirmed the trend for a particular preferential crystallographic orientation depending on periodicity, but, different from sputtered coatings found in the literature, the deposition conditions remained similar with deposition time, ensuring that a consistent value of periodicity was obtained along the entire coating thickness of each deposition process. Another important point of the cathodic arc process is the presence of macroparticles, which have caused local changes in the structure. However, the amount of macro particles, and the associated loss of parallelism of the layers with the coating/substrate interface, has not prevented the use of characterization techniques such as kinematic X-ray diffraction to calculate periodicity based on the position of satellite peaks.

In this work, gas nitrided martensitic stainless steels coupons were PVD-coated using the cathodic arc process. The 30 μm -thick NbN/CrN multilayer coatings were deposited with various periodicities but keeping the same periodicity along the entire coating thickness. The aim of the investigation was to characterize the microstructure, periodicity along all coating thickness and the relationships between microstructure and hardness for such thickness values.

2. Experimental Procedure

NbN-only and CrN-only coatings, as well as NbN/CrN multilayer coatings with different periodicities (Λ varying from 4 to 20 nanometers), were deposited onto gas nitrided martensitic stainless steel (AISI 440B) coupons.

Substrate Preparation and Cleaning - The steel strip was ground and diamond polished, keeping the surface roughness before deposition below $R_z = 0.5 \mu\text{m}$. Before being placed in the deposition chamber, the coupons were chemically cleaned in two different stages. The first stage consisted in the use of a degreasing agent, Renoclean[®] 237, for removal of inorganic and organic residue, while the second stage consisted in ultrasonic rinsing with deionized water.

Coating Deposition - Depositions were conducted in an industrial cathodic arc physical vapor deposition equipment (Hauzer Techno Coating Europe B.V., model HTC750). Figure 1 shows the schematic drawing of the cross section of the equipment displaying the cathode positions. The chamber has three rectangular cathodes (working area of 1200 cm^2), each one capable of working independently and having its own power supply.

The multilayer periodicity was controlled by varying the rotating speed of the table and consequently the time that the specimens pass in front of each target without shield/shutter. The specimens were placed facing the targets in a two-fold rotating table, at a distance of 10 cm from the substrate. The table rotated around the vertical axle of the reactor and each specimen rotated around its own center, to ensure a homogeneous deposition on top of the entire specimen. The rotating speeds were increased 2, 3 and 5

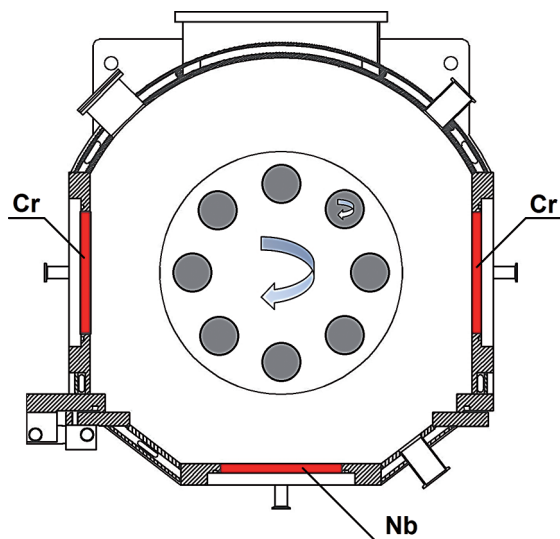


Figure 1: Schematic drawing of the cross section of the HTC-750 coating chamber, showing the target/cathodes positions.

times, leading to the formation of coatings with periodicities of 20 nm, 10 nm, 7.5 nm and 4 nm.

The substrate was heated to 400 °C, a floating bias voltage was applied and the maximum output was 120 W/cm² for each cathode. Before the deposition of the coatings, the substrates were ion cleaned with Cr targets switched on (metal ion cleaning) in Ar atmosphere.

The average deposition rate was 3 µm/h, as detailed below, and the total thickness of the multilayer coatings was 30 µm, in all cases.

The deposition process consisted of three stages:

1. Ion cleaning using a bias voltage of -900 V.
2. Deposition of a metallic chromium bonding layer under argon atmosphere, with total pressure lower than 10⁻³ mbar and using a substrate bias voltage of -20 V.
3. Deposition of multilayer coatings by simultaneous operation of all three targets. During the whole deposition process, the total pressure was kept at 3×10⁻³ mbar and the ratio between argon and nitrogen was kept at 0.25. The electric current applied to niobium and chromium targets was balanced aiming an atomic ratio of Nb/Cr = 0.8. The total time for effective deposition was 9.5 hours.

The superlattice periodicity is controlled by the power dissipated on the targets, the partial pressure of the reactive gas, the bias voltage applied to the substrate and the primary rotation speed of the turntable.

After deposition, cross sections of the coatings were cut with a diamond disk in the preparation for observation, mounted in Bakelite, ground with silicon carbide paper (#120, #320 and #1200) and polished using diamond paste (3 µm and 1 µm).

Measurements of the total thickness of the coatings were conducted using a FEI Quanta 600 – FEG scanning electron microscope. Additionally, qualitative and semi-quantitative chemical composition assessments of all the coatings were carried out using energy-dispersive X-ray spectroscopy (EDS). The crystallographic structures of the multilayer coatings were determined by X-ray diffraction using a Multiflex Rigaku diffractometer. A configuration of Bragg-Brentano θ -2 θ , copper K α radiation (1.5418 Å) and 2 θ angles varying from 20° to 120° with an interval of 0.02° and 2 seconds of integration time per point was used.

The coatings were also characterized by Transmission Electron Microscopy (TEM) for quantitative analysis of the nanostructured multilayer constituents and assessment of their relative thicknesses and diameter of polycrystalline columns. High Resolution Transmission Electron Microscopy (HRTEM) was used to assess a qualitative evaluation of the interfaces between the sub-layers. For this purpose, thin foils were prepared using an FEI Helios 660 Focused Ion Beam (FIB) scanning electron microscope. In order to carry out the TEM analysis across the 30 µm thick coatings, it was used a 200 kV TEM Philips CM20 microscope equipped with an EDS Voyager Noran analyzer (high purity Ge detector and ultra-thin window - UTW). The high resolution images were acquired with a 300 kV HRTEM JEOL 3010. The electron diffraction analysis was conducted following the procedure published by Zuo *et al.*³¹ and provided information about the crystal structure of individual sub-layers (NbN and CrN), the orientation of the (hkl) planes and the preferential direction of crystal growth.

A Micro Combi Tester with instrumented indentation system (maximum normal loads up to 500 mN) and a Hysitron TI950 (30 s load/unload and maximum normal load up to 10 mN) were used to assess the coating microhardness, according to the ISO standard 14577-4 – Edition 2007. The hardness measurements were conducted on the polished coating cross section. The instrumented microindentation results presented in this work are an average of five measurements. The number of nanoindentations in each sample was significantly higher (over 200) and aimed at measuring hardness along the entire coating thickness.

3. Results and Discussion

3.1. Microstructure of single layer coatings (NbN or CrN)

The structure of individual NbN and CrN coatings depends mainly on the nitrogen partial pressure, the bias voltage and the total pressure. Transition metals nitrides exist in different allotropic forms with different stoichiometries. For instance, nitrides composed of Nb and N can present the following chemical compositions and crystalline structures:

β -Nb₂N (hexagonal), γ -Nb₄N₃ (tetragonal), δ -NbN (face-centered cubic), δ' -NbN (hexagonal), ϵ -NbN (hexagonal), η -NbN (hexagonal), and α -Nb(N) a solid solution formed by metallic Nb containing solubilized N¹¹. Additionally, nitrides composed of Cr and N can appear as: CrN (face-centered cubic) and Cr₂N (hexagonal)⁵.

Chromium-based (chromium, CrN, CrC and Cr-C-N) hard coatings produced by PVD have been used successfully in tribological systems where corrosion, oxidation and intense wear are expected. These coatings came out as replacements for electroplated hard chromium in some applications; fcc-CrN coated piston rings, have been used successfully in heavy internal combustion engines. The aim of combining chromium with niobium as the chemically stable metal is to enhance the corrosion resistance of the coating and to increase hardness values to 40 GPa, by utilizing the superlattice effect²⁰. A multilayer coating containing alternate layers of two isostructural phases (fcc - δ -NbN and fcc - CrN) with a small difference in lattice parameter, can give rise to coherency strains/stresses responsible for the strong hardening. Accordingly, NbN/CrN depositions were made with settings chosen to properly obtain δ -NbN (face-centered cubic) and CrN (face-centered cubic) nitrides.

Given that the energy of formation of fcc δ -NbN ($\Delta H^{298} = 56,8$ Kcal/mol) and fcc CrN ($\Delta H^{298} = 29,8$ Kcal/mol) differ significantly, adjustment of the deposition parameters of the cathodic arc process is mandatory in order to allow the formation of a multilayer coating constituted only by the two fcc phases, δ -NbN and CrN. After optimization of the deposition parameters, individual NbN and CrN coatings were produced and analyzed by X-ray diffraction in the θ - 2θ geometry, resulting in the X-ray diffraction patterns shown in Figure 2.

Figure 2 shows that both NbN and CrN phases have a face centered cubic structure with a (200) preferred orientation. The d-spacings are the same as those indicated on ICDD cards #38-1155 and #11-65, respectively, giving lattice parameters of 0.439 nm for NbN and 0.415 nm for CrN, thus producing a difference around 5.5% between the two parameters. These parameters also suggest that there is no nitrogen excess in the coating structures³² and that no significant peak shifts due to coating residual stresses were observed in these cases. The additional lines, visible in the diffraction patterns of NbN refer to Nb droplets. The X-ray diffraction patterns in Figure 2 were considered “standards” for individual NbN and CrN lines that could be used in comparison with those obtained with the multilayer diffraction pattern.

3.2. Microstructure of the multilayer coating

Figure 3 shows a low-magnification photograph of the surface of a 4 nm periodicity coating. The ARC coating process leads to the formation of a significant amount of droplets on the top of the coated surfaces. The use of these

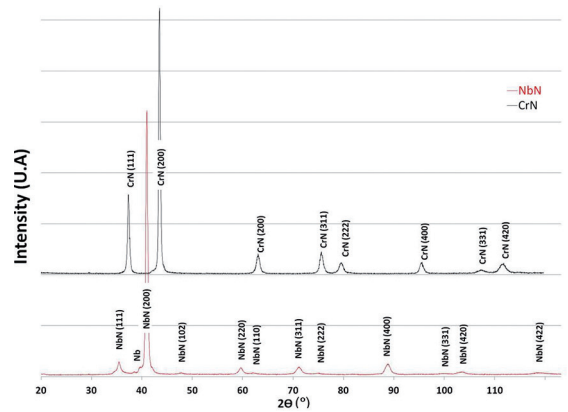


Figure 2: X-ray diffraction patterns of NbN and CrN coatings, containing information about the phases and crystallographic planes.

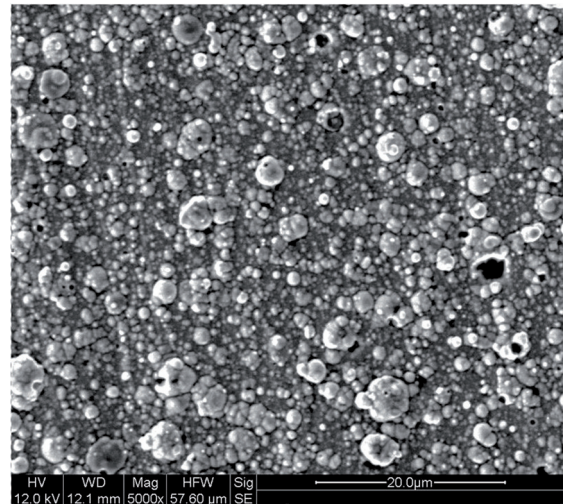


Figure 3: Observation of the coating surface of a 4 nm periodicity coating at low magnification. SEM (SE image).

coatings for tribological applications requires grinding and polishing after deposition. These macroparticles are present during the entire deposition and they can also interfere with the growth of the nanoscale multilayer coating. This was not the case in this work, as detailed later.

Figure 4 shows the Cr bonding layer, with an average thickness of 1 μ m, and its columnar structure. Figure 4 provides preliminary evidence that the NbN/CrN structure is constituted of uniform and well-spaced alternate layers of NbN (light) and CrN (dark). Figure 4 also indicates a dark layer below the chromium layer, most probably formed due to ion etching and chromium diffusion.

Figure 5 shows the θ - 2θ X-ray diffraction patterns for all four NbN/CrN multilayer coatings with different periodicities.

For the 20 nm modulated (periodicity) NbN/CrN coating, it is possible to identify peaks related to NbN and CrN. These peaks are displaced with respect to the correspondent positions of the individual peaks of NbN and CrN in Figure 2.

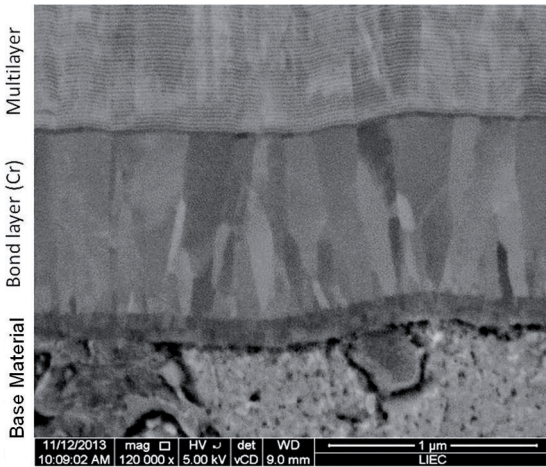


Figure 4: SEM – vCD (low voltage high contrast detector). Detail showing the base material, the chromium bonding layer and the NbN/CrN multilayer coating.

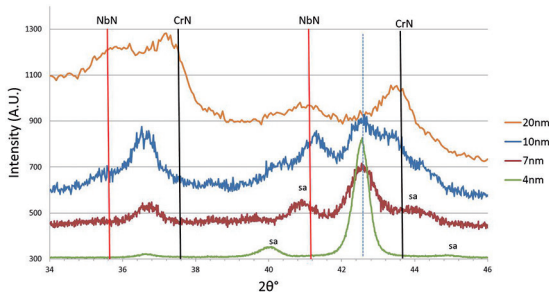


Figure 5: X-ray diffraction patterns of the four NbN/CrN multilayer coatings with periodicities of 4 nm, 7.5 nm, 10 nm and 20 nm. In the same image, the full lines in red and black indicate the positions corresponding to NbN and CrN, ICDD #38-1155 and ICDD #11-65 cards, respectively in the (111) and (200). The dotted line, identified by “I”, corresponds to the intermediate peaks of the 10 nm, 7.5 nm and 4 nm periodicity multilayer coatings. “sa” are the satellite peaks around the central peak in the (200) position.

For the smallest periodicity studied in this work, the lattice parameters of the NbN and CrN sublayers change towards a common intermediate value (Figure 5).

The development of a (200) texture on NbN/CrN coatings can be seen with periodicities smaller than 10 nm, especially for 4 nm periodicity coating. Moreover, the diffraction patterns show a strong central peak, and a group of satellite peaks on its vicinities with gradually decreasing intensities. The central peak is located at $2\theta = 42.5^\circ$, and the first order satellite peaks are visible at both sides of the central peak, as predicted in the literature³³⁻³⁵.

Periodicity and average d-spacings for the coatings thinner than 10 nm were calculated based on the formulation described by Segmüller and Blakeslee³⁶. Following this procedure, equation $2\bar{d}\sin\theta = n\lambda$ identifies Bragg’s central peak position related to the multilayer and $\Lambda = (N_A + N_B)\bar{d}$ determines the modulation period. In these equations, N is the average number of planes and Λ is the periodicity

of two sublayers. The central peak position represents the average d-spacing between the sublayers, corresponding to the weighted average between the d-spacing of each sublayer component, and being calculated using equation 1:

$$\bar{d} = \frac{N_{NbN}d_{NbN} + N_{CrN}d_{CrN}}{N_{NbN} + N_{CrN}} \quad (1)$$

The multilayer modulation period, calculated based on the position of satellite peaks is given by equation (2), where m and n are integers that represent the order of the satellite peaks chosen for Λ calculation

$$\Lambda_{sat} = \frac{|m - n|\lambda}{2|\sin(\theta_m) - \sin(\theta_n)|} \quad (2)$$

The identification of these parameters has been conducted with the help of the program SLERFWIN by G. Gladyszewski³⁷. This software considers the Monte Carlo approach for modelling imperfect multilayers and is based on kinematic X-ray diffraction. The program was used to simulate X-ray patterns, which were latter compared with the diffraction patterns obtained experimentally. Figure 6 presents this comparison for the NbN/CrN sample with a periodicity of 4 nm and 7.5 nm, indicating a good match between simulated and experimental data.

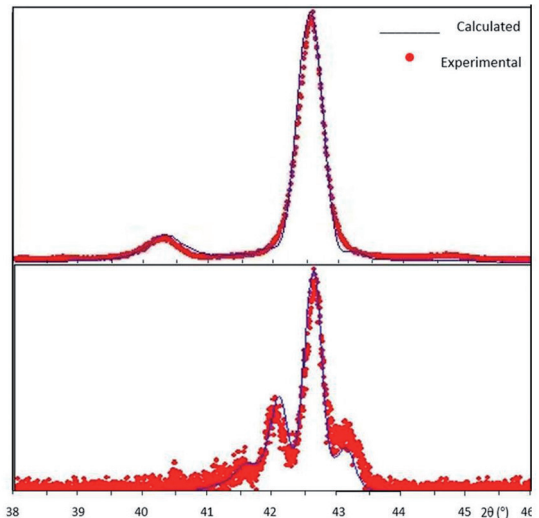


Figure 6: Experimental and calculated (using the SLERFWIN software) X-ray diffraction pattern in the (200) region, for NbN/CrN multilayer samples with a periodicity of 4 nm and 7.5 nm.

Table 1 shows the structural parameters selected for the adjustment shown in Figure 6. Table 1 also presents the calculated periodicity and sub-layer thickness for the 4 nm and 7.5 nm coatings, as well as the values measured (for all specimens) by high-resolution transmission electron microscopy (HRTEM). Comparing the calculated and

Table 1: Periodicity values and sublayers thickness as calculated by the SlerfWin Program for $\Lambda = 4.0$ nm and 7.5 nm) and values measured by HRTEM for Λ from 4 to 20 nm.

	X-Ray (calculated)		HRTEM (measured)			
	4 nm	7.5 nm	4 nm	7.5 nm	10 nm	20 nm
Periodicity	3.6	7.2	4.0	7.7	10.5	20.7
NbN sub-layer (nm)	1.7	3.2	1.9	3.6	4.7	9.6
CrN sub-layer (nm)	1.9	4.0	2.1	4.1	5.8	11.1

experimentally measured values, one can see differences smaller than 10%, indicating a good fit.

The analysis of the microstructures by TEM indicates that all four coatings were formed by deposition of alternate CrN and NbN sublayers with decreasing periodicities of about 20.7 nm, 10.5 nm, 7.7 nm and 4.0 nm. Due to the high total thickness of the coating, the inspection of the whole coating structure was conducted on different areas lying at different depths. It was observed that the sublayers thickness variation along the total coating was smaller than 7%. Thus, the microstructure was found to be homogeneous along the whole coating thickness, confirming that the control of the rotating speed of the table is an effective tool to control the sublayer thickness. In comparison with sputtering-deposited NbN/CrN coatings^{20,23}, the coatings deposited in this work do not present an evident decrease in bi-layer period as the overall thickness increases, Figure 7. This decrease was observed by Lewis²³ and was explained based on: (i) texture development and re-sputtering rate and (ii) target poisoning throughout the process. The consistency of the bi-layer periodicity along the coatings obtained in this work may be a result of (i) not only the characteristics of the cathodic arc process, in which the effect of target poisoning is not comparable with those of the sputtering processes, but also (ii) the use of lower bias voltages (-20 V in comparison with -75 to -150 V).

In addition, a significant technological advantage results from this methodology, since all targets (Niobium and Chromium) work at the same time during the deposition process, optimizing the deposition rate and consequently reducing the coating manufacturing cost. High deposition rates, typical of the cathodic arc process ($\sim 3 \mu\text{m}/\text{h}$ ¹³ against $\sim 1 \mu\text{m}/\text{h}$ for sputtering^{23,29}), were achieved. Moreover, the

deposition parameters selected in this work allowed the deposition of 30 μm thickness coatings, which are much larger than the reported similar multilayer systems below 7 μm ^{20,23}. The deposition of coatings with thickness above 30 μm may be mandatory in some applications; for example, in components for internal combustion engines, which are associated with operations over extended periods of time^{6,7}.

Figure 7 also shows that NbN and CrN sublayers follow the irregularities of the surface of the substrate, as well as those due to the presence of metallic Nb and Cr macroparticles (droplets) deposited during the cathodic arc process. It is noted that these macroparticles affect neither the periodicity nor the individual layer thickness.

The columnar microstructure (with variable column widths between 50 nm and 100 nm) overlaps the multilayer structure maintaining the same orientation by a mechanism of localized epitaxial growth. The width of these columns may increase or decrease along the coating thickness, according to the simultaneous growth rule⁹.

Figure 8 shows a TEM image displaying the multilayers with their respective selected area diffraction patterns. This image indicates that both phases are face-centered cubic (fcc) and textured in the [002] direction.

A double spot can be observed in the area highlighted in Figure 8b, representing the two crystals of the NbN and CrN sublayers. They exhibit similar orientation with slightly different lattice parameters, indicating epitaxial growth of the sublayers.

Figure 9 shows a HRTEM image of the multilayer coating, at the earliest stages of the growth on top of the Cr interlayer. Although there is no parallelism between atomic planes of the Cr interlayer and the first deposited NbN sublayer, parallelism can be observed between the atomic

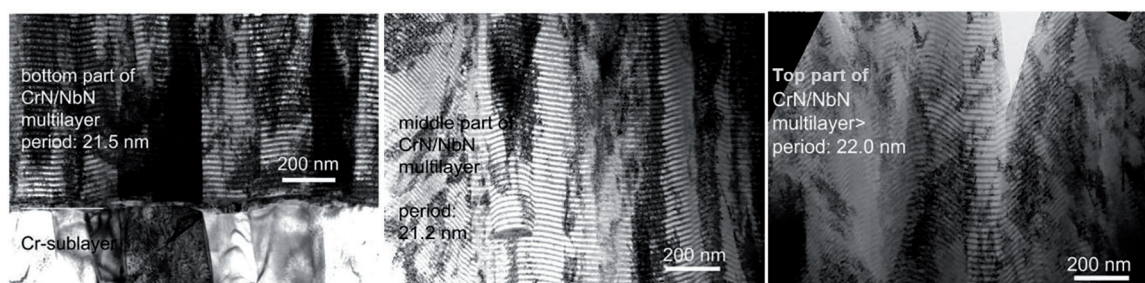


Figure 7: Bright-field micrographs of the cross-section of the NbN/CrN multilayer coating with periodicity of ~ 20 nm taken (a) near the interface; (b) at the middle of the coating and (c) near the surface.

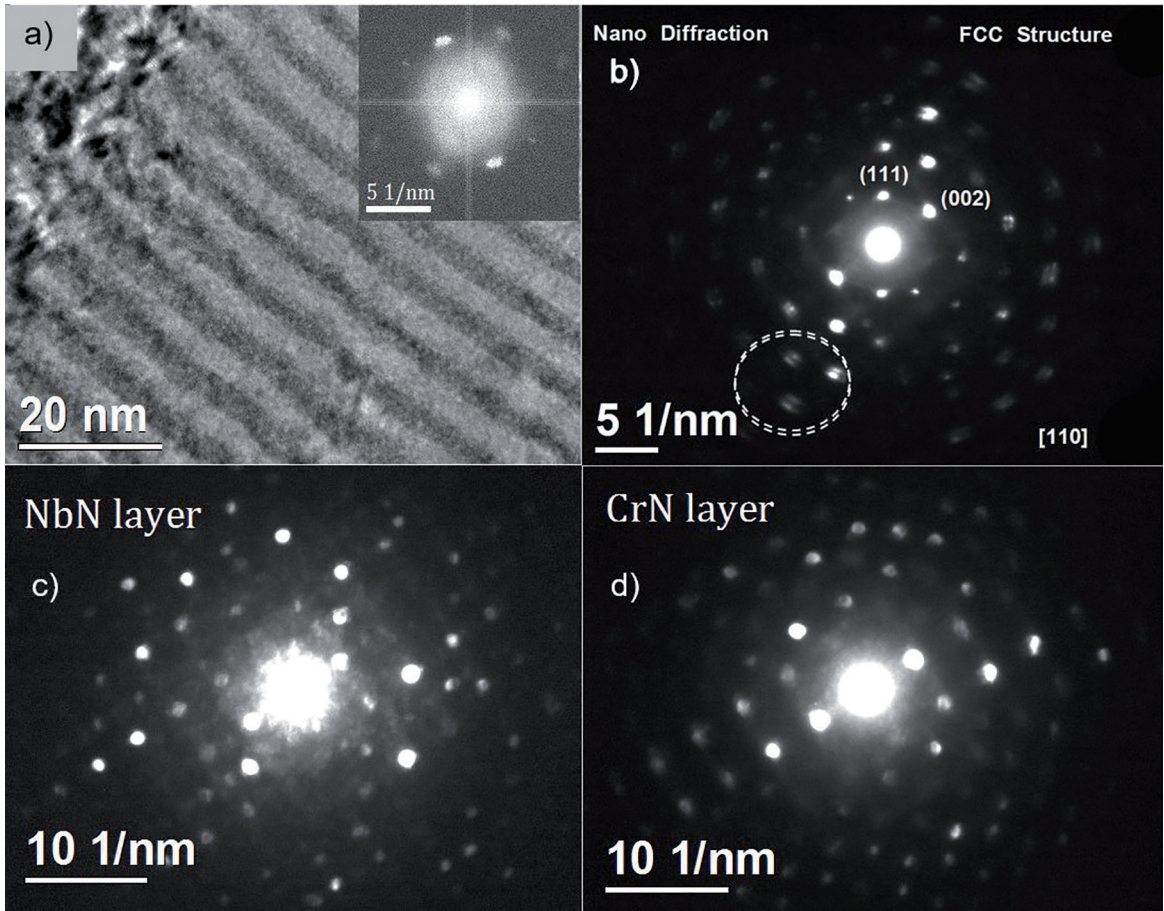


Figure 8: TEM image of a ~10 nm multilayer coating, with its respective Electron diffraction pattern. (a) The micrograph shows the region used for acquiring the diffraction patterns. (b) Electron diffraction pattern obtained from an area (diameter 50 nm) enclosing both NbN and CrN layers and diffraction spots from individual NbN and CrN layers (c and d, respectively).

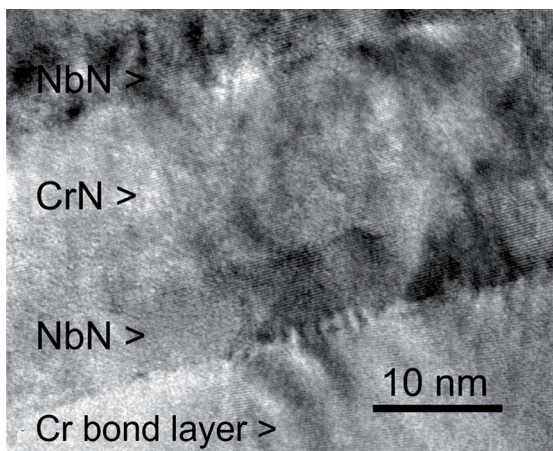


Figure 9: HRTEM image of the multilayer coating, at the earliest stages of growth on top of the Cr interlayer. NbN/CrN coating with periodicity of 20 nm.

planes of the subsequent CrN and NbN sublayers and even localized epitaxy.

The NbN and CrN layers could be related to coherence stresses and hardness, which increases as the periodicity

decreases. Although the presence of metallic Cr and Nb macroparticles caused a disorder in the layer regularity, it was possible to detect the formation of superlattice, satellite peaks on coatings of 7.5 and 4 nm.

3.3. Microhardness and periodicity

Nanohardness measurements were performed along the entire coating thickness, from surface to base material. Figure 10 presents the plotted nanohardness profile along the entire 30 μm thickness of the 20 nm periodicity NbN/CrN. These measurements were performed in order to illustrate that no significant variation in hardness was detected along the thickness of the NbN/CrN multilayer coatings. Local variations in hardness values can be attributed to the presence of macroparticles on the coating.

Since Figure 10 indicates that no hardness variation occurs along the thickness of the NbN/CrN multilayer coatings, microhardness measurements were performed on polished cross sections of multilayer coatings with different periodicities, in order to investigate the effect of the multilayer periodicity on the overall hardness of the coating. The results

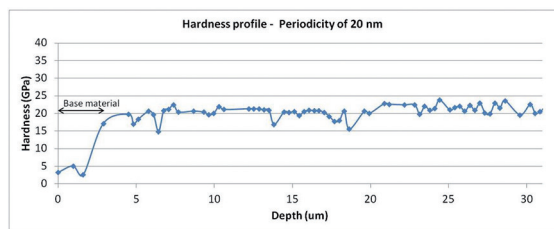


Figure 10: Nanohardness profile of NbN/CrN multilayer coating ($\Lambda = 20$ nm) as a function of coating thickness.

are presented in Figure 11. This plot includes values obtained with specimens with other periodicities than the four detailed in this work, but produced following the same procedure. Figure 11 indicates that hardness increases as the periodicity decreases from 20 nm to 4 nm. This result is in agreement with previous works⁴¹⁻⁴³, which reported hardness values 2-3 times greater for polycrystalline nitride multilayer coating (TiN/NbN) than for those of homogenous TiN and NbN.

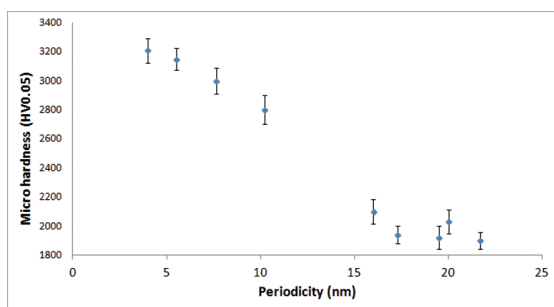


Figure 11: Hardness variation as a function of NbN/CrN multilayer coating bilayer periodicity.

In the 1970's, Koehler suggested that a multilayer coating composed of two different materials with the same crystalline structure would result in a material with very high hardness and toughness, since the interfaces would act as barriers for dislocation movement⁴¹. Some decades later, Sproul *et al.*⁴² stated that several explanations have been proposed to explain the hardness increase, including not only the dislocation barrier due to the interface mismatch⁴³ but also the Hall Petch effect⁴⁴. Additionally, coherent strain and the effect of different modulus of elasticity between sub-layers have been suggested as mechanisms that may contribute for hardness increase. More specifically, Hultman *et al.*⁴⁵ investigated the TiN/NbN system and concluded that plastic deformation and dislocation movement are limited within each sublayer during a scratch test. The hardening effect was once again attributed to the dislocations confinement between the sub-layer interfaces.

Following the concepts presented previously, the hardening effect in multilayer coatings with periodicity around 10 nm and below can be explained by the presence of several sublayers and by the different lattice parameters

of each sublayer. The NbN lattice is around 4% larger than the CrN lattice. The presence of the sublayers forces the crystallographic planes to align, thus reducing the difference between lattice parameters of each sublayer, which is adjusted by elastic stresses. These stresses difficult dislocation movement across the interface. In multilayer coatings with periodicity values greater than 10 nm, the stresses are increasingly relieved within the sublayers, due to the presence of interfacial misfit dislocations and semi-coherent interfaces^{9,46}.

4. Conclusions

NbN/CrN nanostructured multilayers were manufactured by PVD (ARC process). The X-ray analysis combined with computer modeling, allowed the determination of the multilayers periodicity and the d-spacing for NbN and CrN sub-layers. Furthermore, columnar structures with the same crystallographic orientation were formed.

The homogeneity of periodicity throughout the coatings confirms that the deposition rate of CrN and NbN is stable and that the substrate rotation is the main variable in this control. A technological advantage results from this methodology, since both targets (niobium and chromium) work at the same time, improving the deposition rate and reducing the manufacturing cost.

As the coating thickness increases, the sublayer surface becomes more irregular, due to the accumulation of defects and macroparticles. Thus, for engineering applications, surface finishing after coating deposition is required in order to control the roughness.

The modulation periods for those multilayers as determined by X-rays were similar to those measured by Transmission Electronic Microscopy (TEM). When combining the TEM with high angle X-rays analysis, it can be concluded that this last technique is a useful and simple tool to measure the periodicity of nanostructured multilayer coatings, even in coatings prepared by cathodic arc.

The hardness increase observed for the NbN/CrN system is in agreement with the literature, showing that despite the typical discontinuities of the cathodic arc processes, it was possible to take advantage of the combination of nanostructured multilayers.

5. Acknowledgements

The authors acknowledge the financial support from the São Paulo State Research Foundation, FAPESP, processes n. 2012/50890-0, and from National Research Foundation - CNPQ processes n. 481918/2010-8 and 486104/2012-5, to Dr. Carlos Tavares (University of Minho) for his support on X-ray diffraction modelling and analysis and to LNNano – Brazilian Nanotechnology

National Laboratory at CNPEM – Brazilian National Center of Research in Energy and Materials for the Electron Microscopy Measurements.

6. References

1. Aubert A, Gillet R, Gaucher A, Terrat JP. Hard chrome coatings deposited by physical vapour deposition. *Thin Solid Films*. 1983;108(2):165-172.
2. Mayrhofer PH, Willmann H, Mitterer C. Oxidation kinetics of sputtered Cr–N hard coatings. *Surface and Coatings Technology*. 2001;146-147:222-228.
3. Kashiwagi K, Kobayashi K, Masuyama A, Murayama Y. Chromium nitride films synthesized by radio-frequency reactive ion plating. *Journal of Vacuum Science & Technology A*. 1986;4(2):210-214.
4. Ballhause P, Hensel B, Rost A, Schüssler H. CrN_x – a hard coating for corrosion and wear resistance. *Materials Science and Engineering: A*. 1993;163(2):193-196.
5. Friedrich C, Berg G, Broszeit E, Rick F, Holland J. PVD Cr_xN coatings for tribological application on piston rings. *Surface and Coatings Technology*. 1997;97(1-3):661-668.
6. Ferrarese A, Banfield R, Tomanik E. *High value PVD top ring for high speed diesel engines*. SAE Technical Paper 2008-01-0793. Warrendale: SAE International; 2008.
7. Warkentin T, Banfield R, Nocera E. *New ring pack for HDD engines*. SAE Technical Paper 2007-01-2846. Warrendale: SAE International; 2008.
8. Cansever N. Properties of niobium nitride coatings deposited by cathodic arc physical vapor deposition. *Thin Solid Films*. 2007;515(7-8):3670-3674.
9. Münz WD, Lewis DB, Hovsepian PE, Schönjahn C, Ehasarian A, Smith IJ. Industrial scale manufactured superlattice hard PVD coatings. *Surface Engineering*. 2001;17(1):15-27.
10. Ehasarian AP, Wen JG, Petrov I. Interface microstructure engineering by high power impulse magnetron sputtering for the enhancement of adhesion. *Journal of Applied Physics*. 2007;101(5):054301.
11. Reinhard C, Ehasarian AP, Hovsepian PE. CrN/NbN superlattice structured coatings with enhanced corrosion resistance achieved by high power impulse magnetron sputtering interface pre-treatment. *Thin Solid Films*. 2007;515(7-8):3685-3692.
12. Münz WD, Donohue LA, Hovsepian PE. Properties of various large-scale fabricated TiAlN and CrN-based superlattice coatings grown by combined cathodic arc–unbalanced magnetron sputter deposition. *Surface and Coatings Technology*. 2000;125(1-3):269-277.
13. Bemporad E, Pecchio C, Rossi S, Carassiti F. Characterization and wear properties of industrially produced nanoscaled CrN/NbN multilayer coating. *Surface and Coatings Technology*. 2004;188-189:319-330.
14. Tomlinson M, Lyon SB, Hovsepian PE, Münz WD. Corrosion performance of CrN/NbN superlattice coatings deposited by the combined cathodic arc/unbalanced magnetron technique. *Vacuum*. 1999;53(1-2):117-121.
15. Pecchio C, Bemporad E, De Felicis D, De Rossi S, Carassiti F. Production of CrN/NbN superlattice coatings by cathode switching reactive cathodic arc evaporation, International conference on computer methods and experimental measurements for surface treatment effect. In: de Hosson JTM, Brobbia CA, Nishida SI. *Surface Treatment VI - Computer Methods and Experimental Measurements for Surface Treatment Effects*. Southampton: WIT Press; 2003.
16. Setoyama M, Nakayama A, Tanaka M, Kitagawa N, Nomura T. Formation of cubic-AlN in TiN/AlN superlattice. *Surface and Coatings Technology*. 1996;86-87(Pt 1):225-230.
17. Hultman L, Engström C, Odén M. Mechanical and thermal stability of TiN/NbN superlattice of thin films. *Surface and Coatings Technology*. 2000;133-134:227-233.
18. Wadsworth I, Smith IJ, Donohue LA, Münz WD. Thermal stability and oxidation resistance of TiAlN/CrN multilayer coatings. *Surface and Coatings Technology*. 1997;94-95:315-321.
19. Hovsepian PE, Münz WD. Advanced application tailored PVD coatings utilizing nanoscaled multilayer/superlattice structures. In: *Proceedings of the 45th Annual Technical Conference of the Society of Vacuum Coaters*; 2002 Apr 13-18; Lake Buena Vista, FL, USA.
20. Hovsepian PE, Lewis DB, Münz WD, Rouzaud A, Juliet P. Chromium nitride/niobium nitride superlattice coatings deposited by combined cathodic-arc/unbalanced magnetron technique. *Surface and Coatings Technology*. 1999;116-119:727-734.
21. Hovsepian PE, Lewis DB, Münz WD, Lyon SB, Tomlinson M. Combined cathodic arc/unbalanced magnetron grown CrN/NbN superlattice coatings for corrosion resistant applications. *Surface and Coatings Technology*. 1999;120-121:535-541.
22. Hovsepian PE, Lewis DB, Luo Q, Farinotti A. Corrosion resistance of CrN/NbN superlattice coatings grown by various physical vapour deposition techniques. *Thin Solid Films*. 2005;488(1-2):1-8.
23. Lewis DB, Reitz D, Wüstefeld C, Ohser-Wiedemann R, Oette H, Ehasarian A, et al. Chromium nitride/niobium nitride nano-scale multilayer coatings deposited at low temperature by the combined cathodic arc/unbalanced magnetron technique. *Thin Solids Films*. 2006;503(1-2):133-142.
24. Wang HW, Stack MM, Lyons SB, Hovsepian P, Münz WD. The corrosion behaviour of macroparticle defects in arc bond-sputtered CrN/NbN superlattice coatings. *Surface and Coatings Technology*. 2000;126(2-3):279-287.
25. Wang HW, Stack MM, Lyon SB, Hovsepian PE, Münz WD. Wear associated with growth defects in combined cathodic arc/unbalanced magnetron sputtered CrN/NbN superlattice coatings during erosion in alkaline slurry. *Surface and Coatings Technology*. 2000;135(1):82-90.
26. Ceschini L, Lanzoni E, Martini C, Prandstraller D, Sambogna G. Comparison of dry sliding friction and wear of Ti6Al4V alloy treated by plasma electrolytic oxidation and PVD coating. *Wear*. 2008;264(1-2):86-95.

27. Martini C, Ceschini L. A comparative study of the tribological behaviour of PVD coatings on the Ti-6Al-4V alloy. *Tribology International*. 2011;44(3):297-308.
28. Pilone D, Bernabai U. Effect of substrate on wear performance of multilayer hard coating. *Surface Engineering*. 2008;24(3):193-197.
29. Savisalo T, Lewis DB, Luo Q, Bolton M, Hovsepian P. Structure of duplex CrN/NbN coatings and their performance against corrosion and wear. *Surface and Coatings Technology*. 2008;202(9):1661-1667.
30. Araujo JA, Souza RM, Araujo GM, Tschiptschin AP. Effect of periodicity on hardness and scratch resistance of CrN/NbN nanoscale multilayer coating deposited by cathodic arc technique. *Wear*. 2015;330-331:469-477.
31. Zuo JM, Gao M, Tao J, Li BQ, Twesten R, Petrov I. Coherent nano-area electron diffraction. *Microscopy Research and Technique*. 2004;64(5-6):347-355.
32. Vaz F, Ferreira J, Ribeiro E, Rebouta L, Lanceros-Méndez S, Mendes JA, et al. Influence of nitrogen content on the structural, mechanical and electrical properties of TiN thin films. *Surface and Coatings Technology*. 2005;191(2-3):317-323.
33. Thomas O, Gergaud P, Labat S, Barrallier L, Charai A, Alfonso C, et al. Residual Stresses in Metallic Multilayers. *Journal de Physique IV France*. 1996;6(C7):125-134.
34. Tavares CJ, Rebouta L, Rivière JP, Pacaud J, Garemb H, Pischowc K, et al. Microstructure of superhard (Ti,Al)N/Mo multilayers. *Thin Solid Films*. 2001;398-399:397-404.
35. Tavares CJ, Vidrago C, Rebouta L, Rivière JP, Le Bourhis E, Denanot MF. Optimization and thermal stability of TiAlN/Mo multilayers. *Surface and Coatings Technology*. 2005;200(1-4):288-292.
36. Segmüller A, Blakeslee AE. X-ray diffraction from one-dimensional superlattices in GaAs_{1-x}P_x crystals. *Journal of Applied Crystallography*. 1973;6(1):19-25.
37. Gladyszewski G. High resolution studies of interfacial effects by small and large angle X-ray diffraction. *Thin Solid Films*. 1991;204(2):473-484.
38. Chu X, Barnett SA. Model of superlattice yield stress and hardness enhancements. *Journal of Applied Physics*. 1995;77(9):4403-4411.
39. Chu X, Wong MS, Sproul WD, Rohde SL, Barnett SA. Deposition and properties of polycrystalline TiN/NbN superlattice coatings. *Journal of Vacuum Science and Technology A*. 1992;10(4):1604-1609.
40. Shinn M, Hulman L, Barnett SA. Growth, structure and microhardness of epitaxial TiN/NbN superlattices: Journal of Materials Research. 1992;7(4):901-911.
41. Koehler JS. Attempt to Design a Strong Solid, *Physical Review B*. 1970;2(2):547-551.
42. Sproul WD, Yashar PC. Nanometer scale multilayered hard coatings. *Vacuum*. 1999;55(3-4):179-190.
43. Chu X, Barnett SA. Model of superlattice yield stress and hardness enhancements. *Journal of Applied Physics*. 1995;77(1):4403-4411.
44. Anderson PM, Li C. Hall-Petch relations for multilayered materials. *Nanostructured Materials*. 1995;5(3):349-362.
45. Hultman L, Engstrom UC, Oden M, Birch J, Johansson M, Karlsson L. Review of the thermal and mechanical stability of TiN based thin films. *Zeitschrift fur Metallkunde*. 1999;90(10):803-813.
46. Movchan BA, Demchishin AV. Study of the structure and properties of thick vacuum condensates of nickel, titanium, tungsten, aluminum oxide and zirconium oxide. *Physics of Metals and Metallography*. 1969;28(1996):83-90.